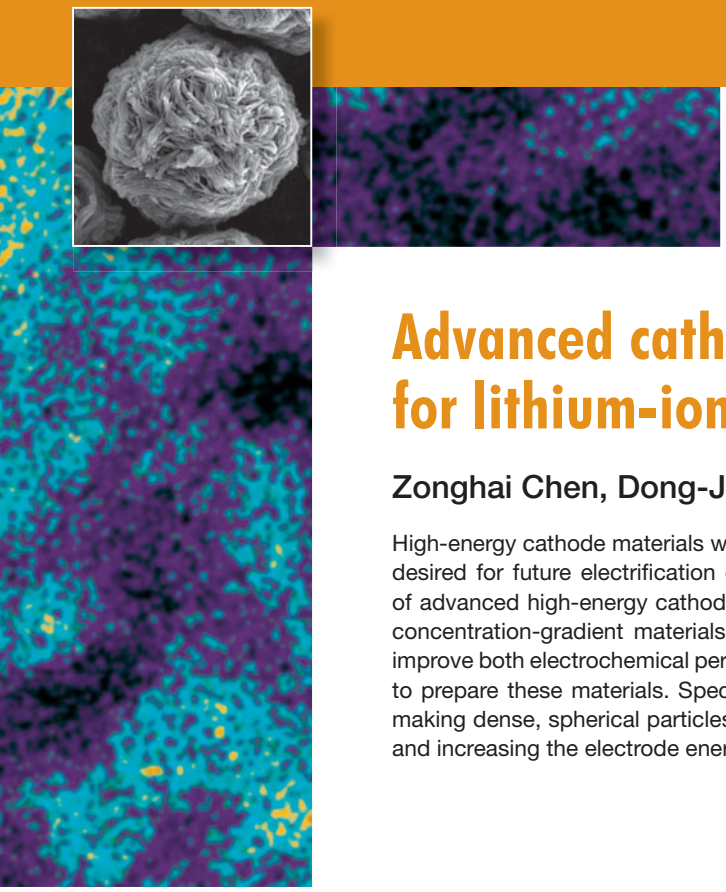


Advanced cathode materials for lithium-ion batteries

Zonghai Chen, Dong-Ju Lee, Yang-Kook Sun, and Khalil Amine

High-energy cathode materials with high working potential and/or high specific capacity are desired for future electrification of vehicles. In this article, we provide a general overview of advanced high-energy cathode materials using different approaches such as core-shell, concentration-gradient materials, and the effects of nanocoatings at the particle level to improve both electrochemical performance and safety. We also summarize the methods used to prepare these materials. Special attention is placed on the co-precipitation process for making dense, spherical particles for the purpose of improving the powder packing density and increasing the electrode energy density.

Introduction

A robust modern economy mainly depends on low-cost, sustainable energy. Currently, the world's energy supply is primarily centered on non-renewable fossil fuels.[1] The energy dilemma facing the world is twofold: global warming from greenhouse gas (CO_2) emission and vulnerability from dependence on depleted supplies of oil. It is projected that world energy consumption will double within the next 50 years, concomitant with worldwide oil production, which will level off in the near future. Moreover, changes in the global economical and political situation inevitably add uncertainty and stress to the world energy supply. An urgent need therefore exists for systematic technological breakthroughs and developments emphasizing energy generation and utilization in order to reduce our reliance upon fossil fuels and to protect the environment. Recently, scientists at Lawrence Livermore National Laboratory published a report on energy consumption that showed that the transportation sector used 71% of the overall petroleum consumed in 2008 in the United States.[2] Because of similar concerns, a worldwide effort has been devoted to developing advanced energy storage technologies for electrification of the transportation system, with the goal of significantly reducing the consumption of fossil fuels. In addition, the development of a low-cost and reliable battery system is critical to enable the utilization of renewable energy sources such as solar and wind energy, whose production period (mostly day time) is separate from the peak consumption period (mostly night time).

After a decade of research, several lithium-ion couples, such as graphite/nano-$LiFePO_4$, nano-$Li_4Ti_5O_{12}$/$Li_{1+x}Mn_{2-x}O_4$, and graphite/$Li_{1+x}Mn_{2-x}O_4$,[3,4] have been reported to meet the requirements for hybrid electric vehicles (HEV).[5] All of these technologies offer high power but limited energy densities, making them inadequate to power pure electric vehicles (EVs) or plug-in hybrid electric vehicles (PHEVs) with an electric drive range of 40 miles. Alternatively, cathode materials made of lithium-rich transition metal oxides with composite structures ($xLi_2MnO_3 \bullet (1-x)LiMO_2$, M is a transition metal or a mixture of transition metals)[6,7] or lithium-rich cathodes ($Li_{1+x}M_{1-x}O_2$, M is a transition metal or a mixture of transition metals)[8,9] offer both higher specific capacity (>200 $mAhg^{-1}$) and higher working potential (>4.3 V versus Li^+/Li). In exchange for their high-energy densities, however, these cathode materials, still in the process of development, require more work to increase their tap density—the amount of material that can be loaded in a specific volume—and to improve their power performance. In addition, this class of materials exhibits capacity fade (or gradually reducing capability to store energy) during cycling or storage at elevated temperatures due to the chemical reaction

Zonghai Chen, Argonne National Laboratory, Argonne, IL 60439, USA; zonghai.chen@anl.gov
Dong-Ju Lee, Hanyang University, Seoul 133-791, Republic of Korea; 2dongju@gmail.com
Yang-Kook Sun, Hanyang University, Seoul 133-791, Republic of Korea; yksun@hanyang.ac.kr
Khalil Amine, Chemical Sciences and Engineering Division, Argonne National Laboratory, Argonne, IL 60439, USA; amine@anl.gov
DOI: 10.1557/mrs.2011.155

© 2011 Materials Research Society
https://doi.org/10.1557/mrs.2011.155 Published online by Cambridge University Press

between the delithiated cathode and the electrolyte at high operating voltage. To overcome the performance degradation of cathode materials and increase their capacity retention when operated at high voltage, several research groups have developed various approaches such as AlF_3 nanocoatings at the particle level in cathodes,[10–19] core-shell structures,[20–30] and a concentration-gradient material.[31–34] All of these materials show higher capacities than conventional cathode materials such as $LiCoO_2$, with further benefits of improved cycling performance and better capacity retention during high temperature storage. In addition, these materials also have higher tolerance to thermal abuse, which is highly desired to ensure safe operation of batteries in a large scale format.

Process to synthesize dense and spherical materials

Many reported processes have been developed to synthesize lithium transition metal oxides, including a sol-gel process,[35–37] spray drying,[38–40] hydroxide-based co-precipitation,[20–26,41–45] and carbonate-based co-precipitation.[7,44] In practice, a high tap density of active electrode materials is highly desired so that more active material can be packed into a specific volume to store more energy. The hydroxide process has been successfully deployed to synthesize a dense and spherical precursor; the spherical morphology is beneficial to reduce the specific surface area of the cathode material that is directly exposed to non-aqueous electrolytes. A small specific surface area is beneficial to minimize the active site for the reaction between the charged cathode material and the electrolyte, and therefore greater stability can be expected. Furthermore, a spherical morphology is preferred for nanoscale coatings and allows for easy and uniform electrode processing.

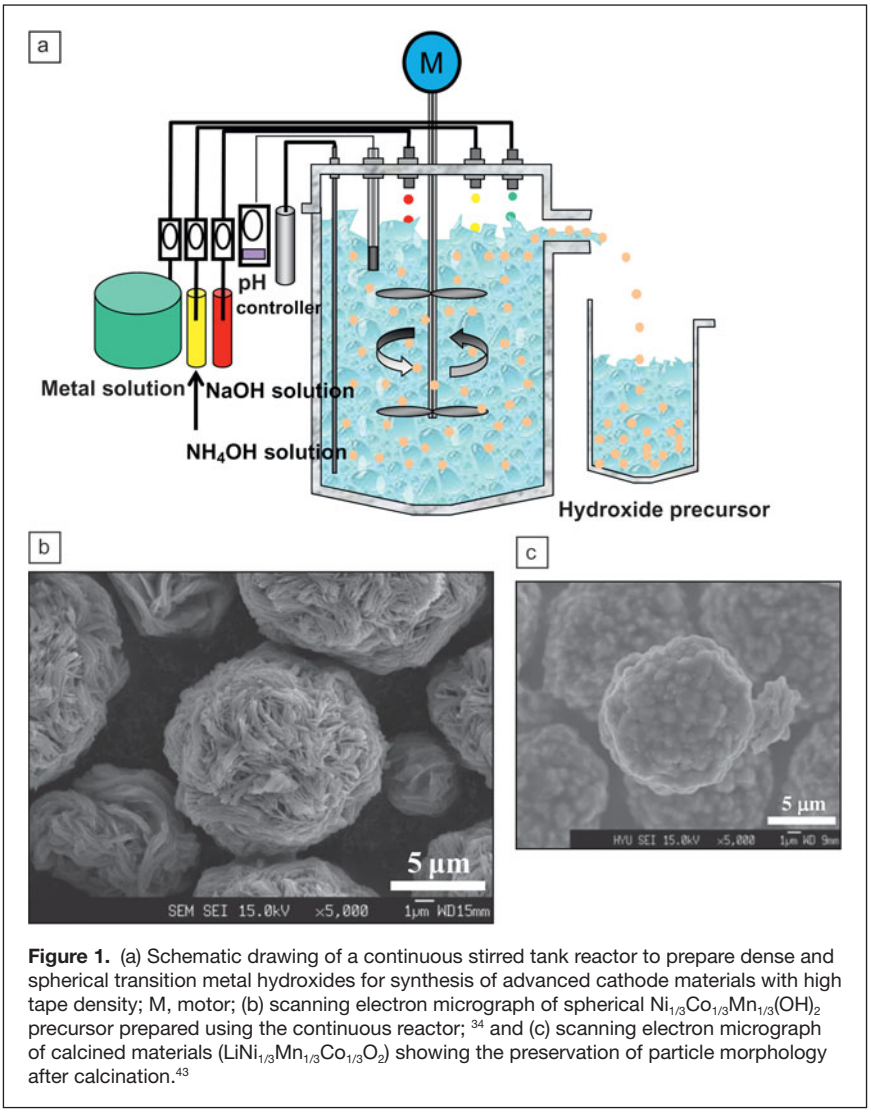


Figure 1. (a) Schematic drawing of a continuous stirred tank reactor to prepare dense and spherical transition metal hydroxides for synthesis of advanced cathode materials with high tape density; M, motor; (b) scanning electron micrograph of spherical $Ni_{1/3}Co_{1/3}Mn_{1/3}(OH)_2$ precursor prepared using the continuous reactor; [34] and (c) scanning electron micrograph of calcined materials ($LiNi_{1/3}Mn_{1/3}Co_{1/3}O_2$) showing the preservation of particle morphology after calcination.[43]

Figure 1a shows a schematic drawing of the continuous stirred tank reactor used in the hydroxide process.[34] This apparatus can also be used for the carbonate process by changing the precipitation agent from ammonium hydroxide solution to Na_2CO_3 or another carbonate source. The continuous reactor has feedback control for both the temperature and pH of the reaction medium and, therefore, has the capability to control the kinetics of particle growth, leading to ideal spherical morphology. Three stock solutions are used in this design: a mixture of the desired transition metal salt dissolved in water, an ammonium solution used as the precipitation agent for the transition metal source, and a NaOH solution used for pH control. The feed rate of the stock solutions can be adjusted to vary the retention time of particles in the reactor tank, providing control of the particle size in the final material. Figure 1b shows a typical scanning electron microscope image of transition metal hydroxides ($Ni_{1/3}Co_{1/3}Mn_{1/3}(OH)_2$) prepared in the continuous stirred tank reactor. After calcination in the presence of a lithium source such as $LiOH{\bullet}H_2O$, the spherical morphology of the metal hydroxide precursor was retained (see Figure 1c).

AlF_3 coating

A lithium-ion battery is sensitive to the operation/storage temperature and its upper cutoff voltage during charge/discharge cycles. To maintain optimal performance, lithium-ion batteries are generally operated below a specific working potential, such as 4.2 V, above which the electrochemical performance suffers greatly.[46] Similar accelerated performance degradation is also widely observed at elevated temperatures, such as 55°C.[46,47] The performance degradation of lithium-ion batteries is thought to partially result from chemical corrosion of the lithium transition metal oxide cathode in the acidic electrolyte. Although a non-aqueous electrolyte is required for lithium-ion batteries, a trace amount of moisture in the range of 20 ppm (parts per million)

https://doi.org/10.1557/mrs.2011.155 Published online by Cambridge University Press

to 100 ppm can still be detected in battery-grade electrolytes. This small amount of moisture tends to react with the main salt ($LiPF_6$) and generate HF, as shown in the following equation:

$$LiPF_6 + H_2O \rightarrow LiF + POF_3 + 2HF. \quad (1)$$

The HF will then slowly corrode the cathode material, causing slow dissolution of the transition metal ion into the electrolyte and migration of this ion to the anode.[48,49] Furthermore, at high voltages, the electrolyte can be easily oxidized because of the high surface oxidation capability of the delithiated oxide.[50,51]

Several surface coating techniques have been widely used to extend the cycle life of lithium transition metal oxide cathodes and to increase their capacity by operating at a higher voltage.[47,52–61] Early efforts were mostly concentrated on metal oxide coatings[47,53–56,60,61] as an HF scavenger to reduce the local acidity (or H^+ concentration) on the surface of cathode materials:

$$2xHF + MO_x \rightarrow xH_2O + MF_{2x}. \quad (2)$$

In Equation 2, M stands for a metal element such as Al, Mg, Zr, or Zn, and x is one half of the valence state of M. The metal-oxide coating has been consistently demonstrated to improve the capacity retention of cathode materials.[47,53–55,60,61] As a typical example of the beneficial effect of Al_2O_3 on the surface of cathode materials, **Figure 2** shows the discharge capacity of bare and Al_2O_3-coated (0.25 wt%) $Li[Li_{0.05}Ni_{0.4}Co_{0.15}Mn_{0.4}]O_2$/C cells at 25°C and 60°C.[55]

Because water is the product of the reaction between HF and the metal oxide coating (see Equation 2), it further reacts with $LiPF_6$ and generates more HF (see Equation 1).The HF then preferably reacts with the nano-metal oxide coating, and thereby delays corrosion of the cathode material. This protection mechanism is lost once the HF completely consumes the protective oxide coating. It is doubtful that the small amount of oxide in the protective shell can persist for the extended period needed for transportation applications (10–15 years). An alternative coating approach is to use a coating that resists HF attack, such as metal fluorides. On the basis of this assumption, AlF_3 was selected as an alternative protective coating of cathode materials.[10–19] Furthermore, Al^{3+} does not oxidize further during cycling at high voltage, and the activation energy of breaking the Al–F bond is very high. As a result, one can expect that the AlF_3 coating will remain intact on the cathode surface during extensive cycling.

Figure 3 shows the x-ray diffraction patterns of uncoated (Figure 3a) and AlF_3 coated cathode materials (Figure 3b) as well as transmission electron micrographs of uncoated (Figure 3c) and AlF_3 coated (Figure 3d) materials. The particular sample in Figure 3 was a delithiated material, $(Li_{0.35}(Ni_{1/3}Co_{1/3}Mn_{1/3})O_2)$,[16] which was first coated with AlF_3 before chemical delithiation. Coating the cathode material with AlF_3 involved precipitation from an aqueous solution of ammonium fluoride and aluminum nitrate. This method resulted in a uniform coating layer that was thinner than 20 nm (see Figure 3d). The x-ray diffraction patterns (Figure 3a and 3b) showed

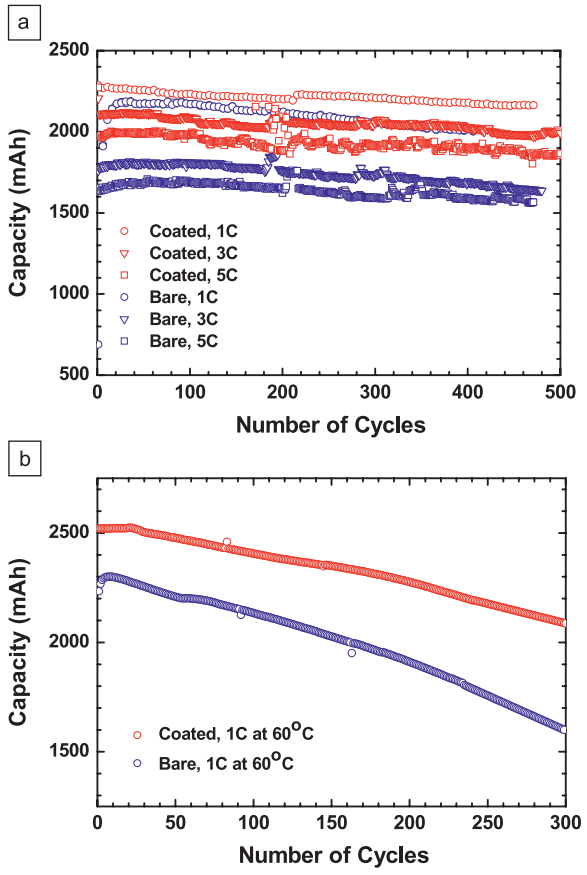


Figure 2. Cyclability of bare and Al_2O_3-coated (0.25 wt%) $Li(Li_{0.05}Ni_{0.4}Co_{0.15}Mn_{0.4})O_2$/C cells at (a) 25°C and (b) 60°C, showing the positive effect of an Al_2O_3 coating on extending cycle life.[55] 1C means to fully charge/discharge the cell in one hour, and 3C means to fully charge/discharge in 20 minutes.

no evidence of the formation of an Al–F-related impurity in the coated material due to the poor crystallinity and the small amount of AlF_3 coating. Rietveld refinement, a method that involves refining powder diffraction data to find the crystal structure, of the x-ray diffraction patterns showed no change in the lattice parameter of the cathode material with and without AlF_3 coating, suggesting that the AlF_3 compound is only present on the surface of the active material.

Figure 4 shows the discharge capacity of Li/pristine and AlF_3-coated $Li(Ni_{1/3}Co_{1/3}Mn_{1/3})O_2$ cells over 50 cycles in the voltage range of 3.0–4.5 V and 3.0–4.6 V at a current rate of 80 $mAh \cdot g^{-1}$ (0.5C rate, or a rate to fully charge/discharge the cell in two hours).[11] In the 3.0–4.5 V range, the pristine and AlF_3-coated $Li(Ni_{1/3}Co_{1/3}Mn_{1/3})O_2$ delivered the same discharge capacity of 173 $mAh \cdot g^{-1}$. The pristine $Li(Ni_{1/3}Co_{1/3}Mn_{1/3})O_2$ showed a gradual decrease in capacity, leading to a capacity retention of 75% after 50 cycles. The AlF_3-coated $Li(Ni_{1/3}Co_{1/3}Mn_{1/3})O_2$ showed a remarkably better capacity retention of 93% for the same cycling period. Similar to the 3.0–4.5 V range, the capacity retention of AlF_3-coated $Li(Ni_{1/3}Co_{1/3}Mn_{1/3})O_2$ in the 3.0–4.6 V range significantly

https://doi.org/10.1557/mrs.2011.155 Published online by Cambridge University Press

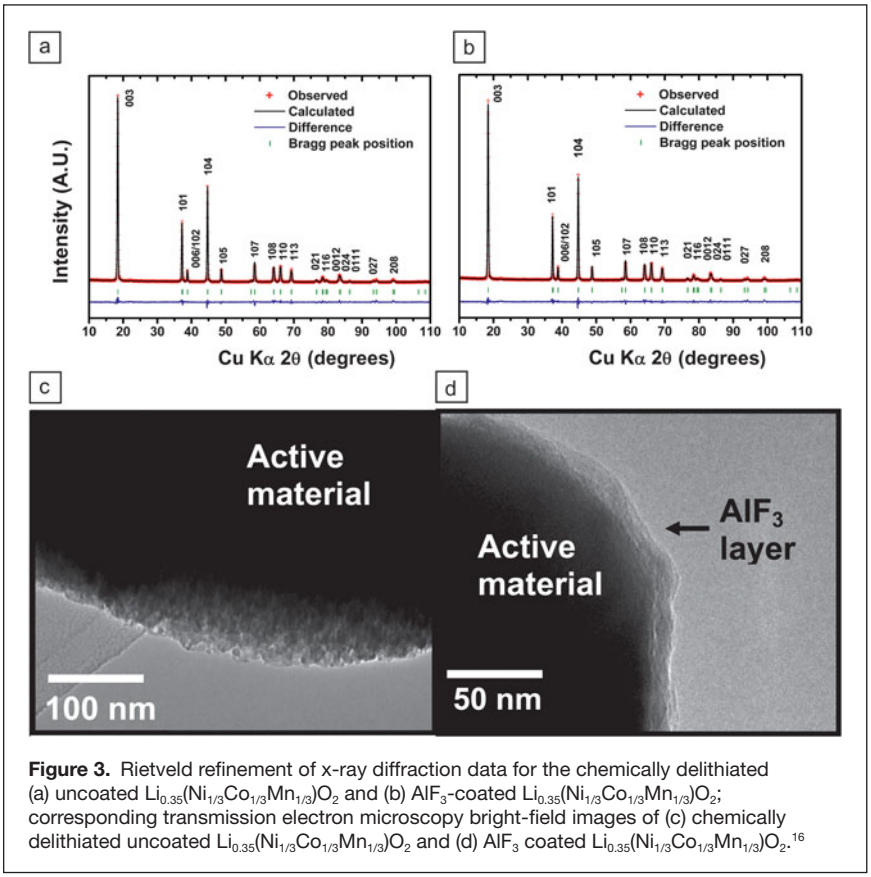


Figure 3. Rietveld refinement of x-ray diffraction data for the chemically delithiated (a) uncoated $Li_{0.35}(Ni_{1/3}Co_{1/3}Mn_{1/3})O_2$ and (b) AlF_3-coated $Li_{0.35}(Ni_{1/3}Co_{1/3}Mn_{1/3})O_2$; corresponding transmission electron microscopy bright-field images of (c) chemically delithiated uncoated $Li_{0.35}(Ni_{1/3}Co_{1/3}Mn_{1/3})O_2$ and (d) AlF_3 coated $Li_{0.35}(Ni_{1/3}Co_{1/3}Mn_{1/3})O_2$.[16]

improved (92% capacity retention) compared to the pristine cathode (72% capacity retention).

Further investigation revealed that the performance of cathode materials also greatly depends on the amount of AlF_3 coating.[12] Overly thick coatings of AlF_3 on $LiCoO_2$ deteriorated both the capacity retention and rate capability of AlF_3-coated $LiCoO_2$[11] thought to be due to the high interfacial impedance of the electrode caused by the thick coating. Another possible explanation is that AlF_3 is an insulator to both electrons and lithium ions, and a thicker coating lowers the kinetics of the charge-transfer reaction at the coating/active material interface. Therefore, an optimum AlF_3 coating is required to achieve a performance that is a compromise between overall protection and charge-transfer kinetics.

Core-shell structured materials

The core-shell structure is a conceptual extension of the AlF_3 coating, where the AlF_3 is replaced by a layer of active cathode material with better thermal stability and better compatibility toward nonaqueous electrolytes.[20–30] In this case, a high-capacity nickel-rich cathode material can be used as the bulk (core), and a nickel-poor composition can be used as the shell. Formation of this core-shell structure has three main steps (**Figure 5**). First, the nickel-rich $(Ni_{0.8}Co_{0.1}Mn_{0.1})(OH)_2$ precursor is formed as the core, with a particle diameter of about 12–13 μm (Step 1). The core is then completely encapsulated by a nickel-poor $(Ni_{0.5}Mn_{0.5})(OH)_2$ shell with a thickness between 1 and 1.5 μm (Step 2). Finally, calcination of the core-shell hydroxide with a lithium salt generates spherical core-shell $Li[(Ni_{0.8}Co_{0.1}Mn_{0.1})_{1-x}(Ni_{0.5}Mn_{0.5})_x]O_2$ powders (Step 3).

The **Figure 6** inset (bottom right) shows a scanning electron microscopy image of the cross-section of the core $LiNi_{0.8}Co_{0.1}Mn_{0.1}O_2$ material, which exhibits capacity fade when operating at high voltage because of high surface reactivity toward the electrolyte. The Figure 6 inset (bottom left) shows the cross-section of the core-shell, where the core and shell are clearly visible. In this case, the core material is $LiNi_{0.8}Co_{0.1}Mn_{0.1}O_2$, and the shell is $LiNi_{0.5}Mn_{0.5}O_2$. The core-shell structure takes advantage of both the high capacity of the core material and the excellent stability of the shell

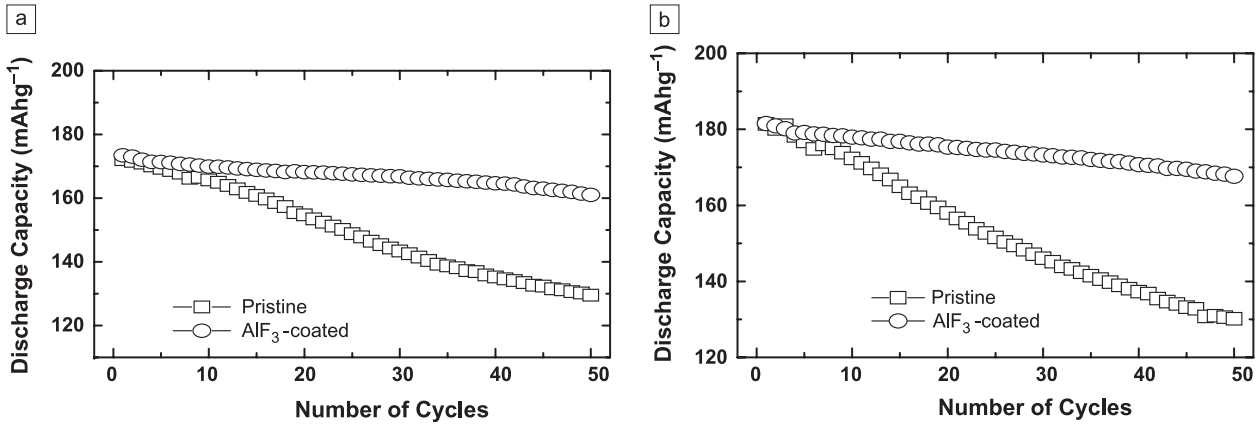


Figure 4. Cycling performance of Li/pristine $Li(Ni_{1/3}Co_{1/3}Mn_{1/3})O_2$ and Li/AlF_3-coated $Li(Ni_{1/3}Co_{1/3}Mn_{1/3})O_2$ cells cycled at (a) 3.0–4.5 V and (b) 3.0–4.6 V show the beneficial impact of the AlF_3 coating on the capacity retention.[11]

https://doi.org/10.1557/mrs.2011.155 Published online by Cambridge University Press

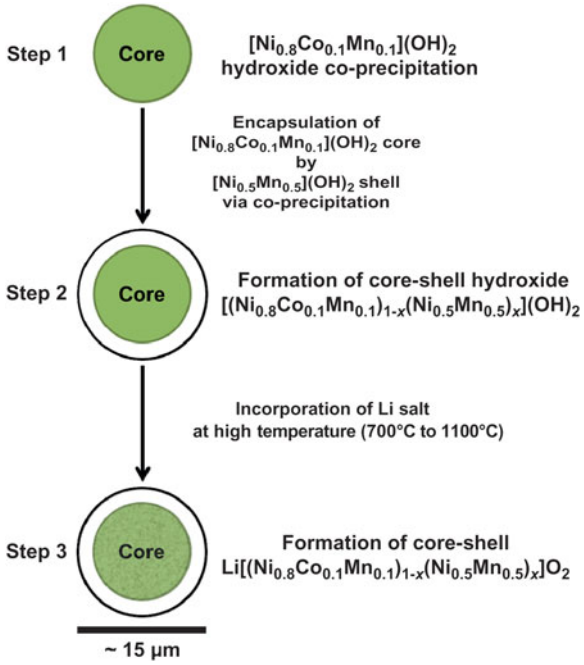


Figure 5. Schematic drawing of the formation process of microscale core-shell structured $Li[(Ni_{0.8}Co_{0.1}Mn_{0.1})_{1-x}(Ni_{0.5}Mn_{0.5})_x]O_2$. Step 1: synthesis of Ni-rich $[Ni_{0.8}Co_{0.1}Mn_{0.1}](OH)_2$; Step 2: formation of core-shell $[(Ni_{0.8}Co_{0.1}Mn_{0.1})_{1-x}(Ni_{0.5}Mn_{0.5})_x](OH)_2$ hydroxide precursor; and Step 3: formation of core-shell $Li[(Ni_{0.8}Co_{0.1}Mn_{0.1})_{1-x}(Ni_{0.5}Mn_{0.5})_x]O_2$ by calcination of $[(Ni_{0.8}Co_{0.1}Mn_{0.1})_{1-x}(Ni_{0.5}Mn_{0.5})_x](OH)_2$ with lithium salt.[20]

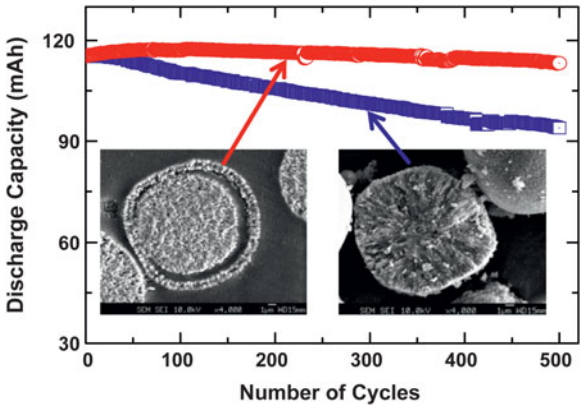


Figure 6. Discharge capacity of lithium-ion cells using a graphite anode and two different cathodes. One of the cathodes is core-shell structured $Li[(Ni_{0.8}Co_{0.1}Mn_{0.1})_{0.8}(Ni_{0.5}Mn_{0.5})_{0.2}]O_2$ (red curve), and the other is $LiNi_{0.8}Co_{0.1}Mn_{0.1}O_2$ (blue curve).[20] The core-shell structure material has better capacity retention than the core material.

material. As a result, the full cell based on the core-shell cathode and a mesocarbon microbead anode shows far better capacity retention with almost no capacity fade after 500 cycles.[20,22]

Figure 7 shows that the core-shell $Li[(Ni_{0.8}Co_{0.1}Mn_{0.1})_{0.8}(Ni_{0.5}Mn_{0.5})_{0.2}]O_2$ has a higher exothermic onset temperature than the core-only $Li(Ni_{0.8}Co_{0.1}Mn_{0.1})O_2$ electrode. A high onset

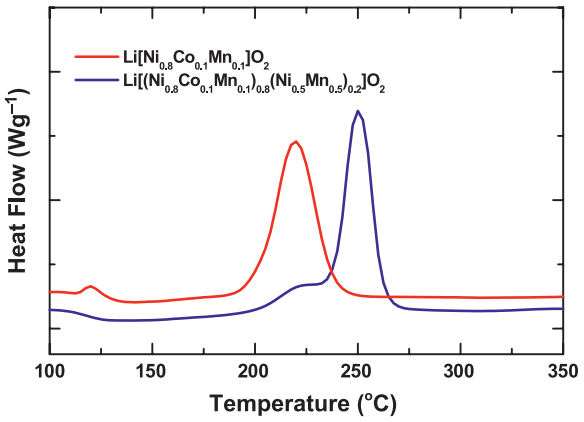


Figure 7. Differential scanning calorimetry traces of $Li[(Ni_{0.8}Co_{0.1}Mn_{0.1})_{0.8}(Ni_{0.5}Mn_{0.5})_{0.2}]O_2$ and $Li[Ni_{0.8}Co_{0.1}Mn_{0.1}]O_2$ charged to 4.3 V show that the core-shell structure material has better thermal stability than the core material.[20]

temperature here generally means higher thermal stability, or, in other words, thermal decomposition of the cathode material will be triggered at a higher temperature. For the $Li(Ni_{0.8}Co_{0.1}Mn_{0.1})O_2$ electrode, the onset temperature of the exothermic peak was about 180°C, above which an abrupt exothermic reaction occurred with an enthalpy of 3285 Jg^{-1} at about 220°C. However, core-shell $Li[(Ni_{0.8}Co_{0.1}Mn_{0.1})_{0.8}(Ni_{0.5}Mn_{0.5})_{0.2}]O_2$ showed an exothermic reaction at 250°C with a reduced enthalpy of 2261 Jg^{-1} when compared to the $Li(Ni_{0.8}Co_{0.1}Mn_{0.1})O_2$ core electrode. As previously reported, the exothermic reaction of $Li(Ni_{0.5}Mn_{0.5})O_2$ occurs at about 270–280°C,with an even lower heat flow.[62] The thermally stable outer $Li(Ni_{0.5}Mn_{0.5})O_2$ shell is believed to suppress the oxygen release from the highly delithiated $Li_{1-x}(Ni_{0.8}Co_{0.1}Mn_{0.1})O_2$, thereby improving the thermal stability of the $Li[(Ni_{0.8}Co_{0.1}Mn_{0.1})_{0.8}(Ni_{0.5}Mn_{0.5})_{0.2}]O_2$ core-shell.

While the core-shell approach improves the electrochemical performance and thermal stability of cathodes, the long-term cyclability of this material is still questionable. Voids of tens of nanometers between the core and the shell of core-shell-structured materials develop during cell testing because of the crystal structure mismatch during cycling.[31] The core material ($LiNi_{0.8}Co_{0.1}Mn_{0.1}O_2$) tends to shrink by approximately 9–10% in volume, while the shell material ($LiNi_{0.5}Mn_{0.5}O_2$) only shrinks by about 3 vol% during cycling. Repeated charge/discharge cycling can cause mechanical stress at the interface between the core and the shell. This stress can lead to fatigue of the material and separation between the core and the shell material, resulting in a significant rise in cell impedance.

Concentration-gradient materials

To avoid cracks between the core material and the shell material in the core/shell structure, Sun and Amine[31–34] reported a novel high-capacity and safe cathode material with Ni-rich layered oxides, in which each particle consists of bulk material surrounded by a concentration-gradient outer layer. As illustrated

https://doi.org/10.1557/mrs.2011.155 Published online by Cambridge University Press

in **Figure 8**, as one example,[31] the bulk is a nickel-rich layered oxide ($Li[Ni_{0.8}Co_{0.1}Mn_{0.1}]O_2$) to satisfy the need for high energy density. In the outer layer, the reactive nickel ions are gradually replaced with manganese ions when moving outward to provide better stability against the electrolyte and improve cycle life and safety. The resulting surface composition is $Li[Ni_{0.46}Co_{0.23}Mn_{0.31}]O_2$, which is much more stable when in contact with the electrolyte than is the bulk composition.

This concentration gradient was prepared by first making a concentration-gradient hydroxide precursor. The core of the precursor, $(Ni_{0.8}Co_{0.1}Mn_{0.1})(OH)_2$, was synthesized with a co-precipitation method using $NiSO_4 \cdot 6H_2O$, $CoSO_4 \cdot 7H_2O$, and $MnSO_4 \cdot 5H_2O$ (8:1:1 in molar ratio) as starting materials. During the reaction, a Ni-poor aqueous solution (Ni:Co:Mn = 0.08:0.46:0.46 in molar ratio) was pumped into a Ni-rich (Ni:Co:Mn = 0.8:0.1:0.1 in molar ratio) solution tank, after which the homogeneously mixed solution was fed into a continuously stirred tank reactor. The obtained particles were filtered, washed with deionized water, and dried at 25°C to remove adsorbed water in a vacuum. **Figure 9** shows cross-sectional scanning electron microscope images and electron probe x-ray microanalysis (EPMA) results of the precursor (Figure 9a and 9c) and concentration-gradient materials (Figure 9b and 9d). The EPMA examination (Figure 9d) showed that the concentration-gradient layer was maintained after calcination, even though the concentration-gradient change of transition metals is less steep than in the case of the hydroxide precursor due to inter-diffusion of metal ions during the high-temperature calcination process.

Figure 10a shows the capacity retention of half cells using $Li(Ni_{0.8}Co_{0.1}Mn_{0.1})O_2$, $Li(Ni_{0.46}Co_{0.23}Mn_{0.31})O_2$, and the concentration-gradient $Li(Ni_{0.64}Co_{0.18}Mn_{0.18})O_2$. The cells were charged to 4.4 V and cycled at 55°C. Cells based on both $Li(Ni_{0.8}Co_{0.1}Mn_{0.1})O_2$ and the concentration-gradient material show a high initial capacity of approximately 209 $mAhg^{-1}$, which would meet the energy requirement needed for PHEVs. However, the cell based on the bulk $Li(Ni_{0.8}Co_{0.1}Mn_{0.1})O_2$ composition retained only 67% of its initial capacity after 50 cycles, whereas the concentration-gradient material showed an excellent capacity retention of 96% during the same cycling period. The capacity retention of the concentration-gradient

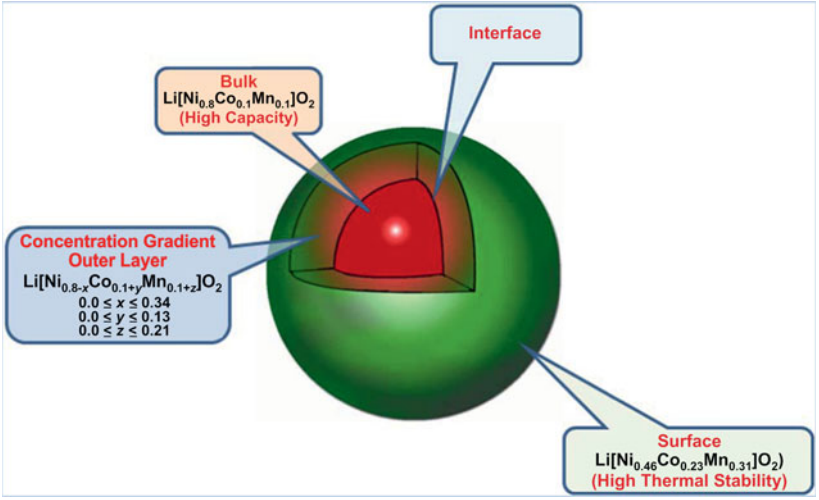


Figure 8. Schematic diagram of a cathode particle with a Ni-rich core surrounded by a concentration-gradient outer layer.[31]

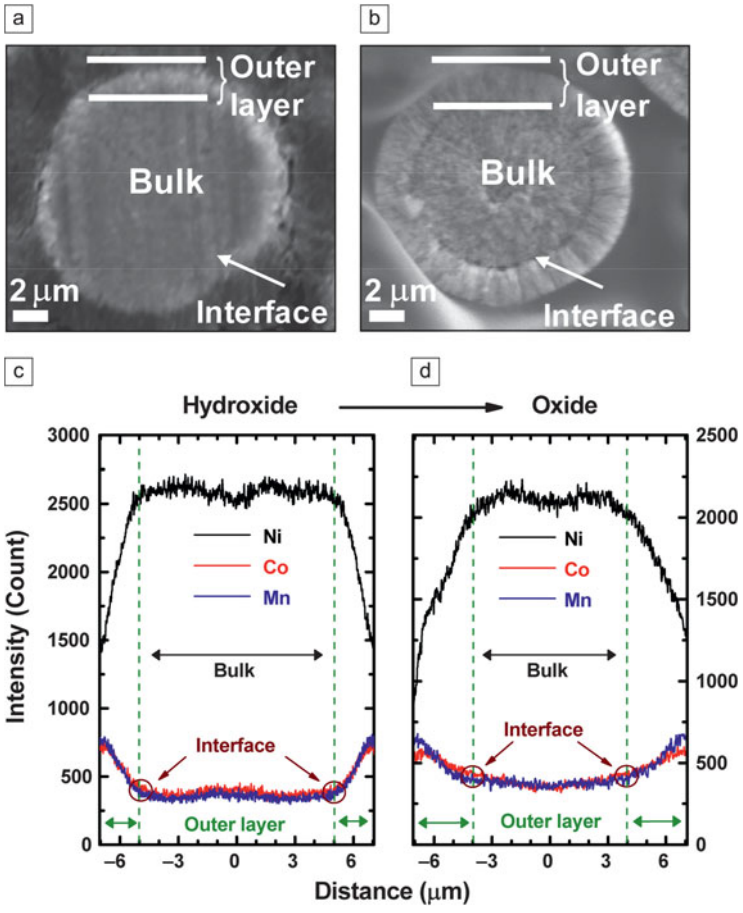


Figure 9. Scanning electron micrograph (a) and electron probe microanalysis (EPMA) line scan (c) of precursor hydroxide; scanning electron micrograph (b) and EPMA line scan (d) of final lithiated oxide $Li[Ni_{0.64}Co_{0.18}Mn_{0.18}]O_2$. In both materials, the gradual concentration changes of Ni, Mn, and Co in the interlayer are clearly evident. The Ni concentration decreases, and the Co and Mn concentrations increase toward the surface.[31]

https://doi.org/10.1557/mrs.2011.155 Published online by Cambridge University Press

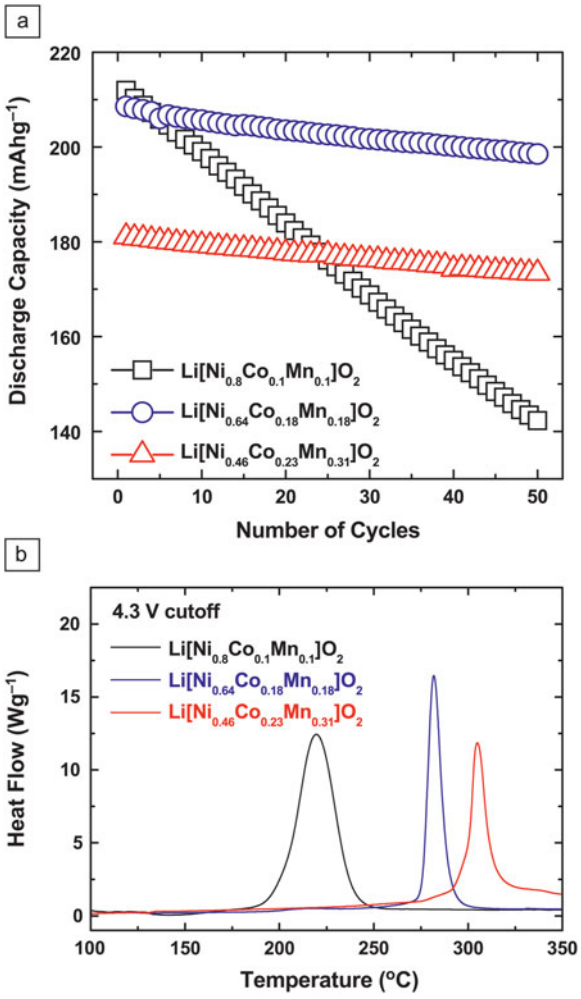


Figure 10. (a) Cycling performance of half cells based on $Li[Ni_{0.8}Co_{0.1}Mn_{0.1}]O_2$, $Li[Ni_{0.46}Co_{0.23}Mn_{0.31}]O_2$, and concentration-gradient material ($Li[Ni_{0.64}Co_{0.18}Mn_{0.18}]O_2$) cycled between 3.0 and 4.4 V at 55°C by applying a constant current of 95 mAg^{-1} (0.5C-rate); (b) differential scanning calorimetry traces showing heat flow from the reaction of the electrolyte with concentration-gradient $Li_{1-x}[Ni_{0.8}Co_{0.1}Mn_{0.1}]O_2$, $Li_{1-x}[Ni_{0.64}Co_{0.18}Mn_{0.18}]O_2$ and $Li_{1-x}[Ni_{0.46}Co_{0.23}Mn_{0.31}]O_2$ charged to 4.3 V. [31]

material is similar to that of the cell based only on the surface composition, $Li(Ni_{0.46}Co_{0.23}Mn_{0.31})O_2$.This result clearly indicates that the concentration-gradient approach can create a composite material that takes advantage of the high energy density of the core and the better stability of the shell.

Figure 10b shows the differential scanning calorimetry profiles of $Li_{1-x}(Ni_{0.8}Co_{0.1}Mn_{0.1})O_2$ and the concentration-gradient $Li_{1-x}(Ni_{0.64}Co_{0.18}Mn_{0.18})O_2$ charged to 4.3 V in the presence of a commonly used electrolyte, 1.0 M $LiPF_6$/ethylene carbonate–diethyl carbonate. For $Li_{1-x}(Ni_{0.8}Co_{0.1}Mn_{0.1})O_2$, the onset temperature of the exothermic reaction occurred at approximately 180°C, with a peak at 220°C.The concentration-gradient material exhibits a higher onset temperature compared with the bulk composition $Li(Ni_{0.8}Co_{0.1}Mn_{0.1})O_2$.The stability of this material may originate from the Mn^{4+} in the surface region. The onset temperature of the exothermic reaction was 270°C for the concentration-gradient $Li_{1-x}(Ni_{0.64}Co_{0.18}Mn_{0.18})O_2$; thus, the reaction with the electrolyte was delayed by approximately 90°C compared with $Li_{1-x}(Ni_{0.8}Co_{0.1}Mn_{0.1})O_2$, owing to the high stability of the outer surface composition $Li_{1-x}(Ni_{0.46}Co_{0.23}Mn_{0.31})O_2$ in the concentration-gradient material, which shows an onset temperature of over 305°C.

Conclusions

The energy density of cathode materials for lithium-ion batteries can be greatly increased by increasing the Ni content, but this increase leads to deteriorated electrochemical and thermal stability of materials in the charged state due to the instability of tetravalent nickel in the oxide phase. Thus, developing cathode materials with high energy density and good stability for transportation applications is a major challenge. As summarized here, this challenge can be mitigated by surface coatings, including strategies such as coating with a thin metal fluoride layer, creating a core-shell structure, and designing concentration-gradient materials. Because of lattice mismatch during charge/discharge cycles, materials with the core-shell structure commonly suffer from mechanical stress between the core and the shell, potentially leading to possible separation at the interface with negative consequences for charge-carrier mobility into the active core. Alternatively, materials designed with a concentration-gradient have better mechanical stability because of the gradual change in the composition, which suppresses lattice mismatch across the particles during charge/discharge cycling. In addition, a common advantage of these surface coating techniques is that the coating layer is inert or less reactive toward non-aqueous electrolytes, resulting in an improvement in the electrochemical performance and the thermal stability of the cathode material.

Acknowledgments

The research of Z. Chen and K. Amine is funded by the U.S. Department of Energy, FreedomCAR, and Vehicle Technologies Office. Argonne National Laboratory is operated for the U.S. Department of Energy by the UChicago Argonne, LLC, under contract DE-AC02-06CH11357. The work of D.-J. Lee and Y.-K. Sun was supported by the Basic Science Research Program through the National Research Foundation of Korea (NRF) grant funded from the Ministry of Education, Science and Technology (MEST) of Korea for the Center for Next Generation Dye-sensitized Solar Cells (No. 2010-0001842) and by the Human Resources Development of the Korea Institute of Energy Technology Evaluation and Planning (KETEP) grant funded by the Korea government Ministry of Knowledge Economy (No. 20104010100560).

References

1. J.B. Goodenough, H.D. Abruña, M.V. Buchanan, *Basic Research Needs for Electrical Energy Storage: Report of the Basic Energy Sciences Workshop on Electrical Energy Storage* (U.S. Department of Energy, Office of Basic Energy Sciences, Washington, DC, 2007).
2. Lawrence Livermore National Laboratory; https://www.llnl.gov/news/newsreleases/2009/NR-09-07-02.html?snc=15601.
3. S.Y. Chung, J.T. Bloking, Y.M. Chiang, *Nat. Mater.* **1**, 123 (2002).

https://doi.org/10.1557/mrs.2011.155 Published online by Cambridge University Press

4. K. Amine, I. Belharouak, Z.H. Chen, T. Tran, H. Yumoto, N. Ota, S.T. Myung, Y.-K. Sun, *Adv. Mater.* **22**, 3052 (2010).
5. U.S. Department of Energy, *Partnership of New Generation Vehicle Battery Test Manual*, revision 3, DOE/ID-10597 (2001).
6. J.S. Kim, C.S. Johnson, J.T. Vaughey, M.M. Thackeray, S.A. Hackney, *Chem. Mater.* **16**, 1996 (2004).
7. H.X. Deng, I. Belharouak, R.E. Cook, H.M. Wu, Y.-K. Sun, K. Amine, *J. Electrochem. Soc.* **157**, A447 (2010).
8. Z. Lu, D.D. MacNeil, J.R. Dahn, *Electrochem. Solid-State Lett.* **4**, A192 (2001).
9. Z.H. Lu, J.R. Dahn, *J. Electrochem. Soc.* **149**, A1454 (2002).
10. Y.-K. Sun, J.-M. Han, S.-T. Myung, S.-W. Lee, K. Amine, *Electrochem. Commun.* **8**, 821 (2006).
11. Y.-K. Sun, S.-W. Cho, S.-W. Lee, C.S. Yoon, K. Amine, *J. Electrochem. Soc.* **154**, A168 (2007).
12. Y.-K. Sun, S.-W. Cho, S.-T. Myung, K. Amine, J. Prakash, *Electrochim. Acta* **53**, 1013 (2007).
13. H.-B. Kim, B.-C. Park, S.-T. Myung, K. Amine, J. Prakash, Y.-K. Sun, *J. Power Sources* **179**, 347 (2008).
14. B.-C. Park, H.-B. Kim, S.-T. Myung, K. Amine, I. Belharouak, S.-M. Lee, Y.-K. Sun, *J. Power Sources* **178**, 826 (2008).
15. Y.-K. Sun, C.S. Yoon, S.-T. Myung, I. Belharouak, K. Amine, *J. Electrochem. Soc.* **156**, A1005 (2009).
16. S.-T. Myung, K.-S. Lee, C.S. Yoon, Y.-K. Sun, K. Amine, H. Yashiro, *J. Phys. Chem. C* **114**, 4710 (2010).
17. H. Deng, I. Belharouak, C.S. Yoon, Y.-K. Sun, K. Amine, *J. Electrochem. Soc.* **157**, A1035 (2010).
18. H.C. Lin, J.M. Zheng, Y. Yang, *Mater. Chem. Phys.* **119**, 519 (2010).
19. J.M. Zheng, Z.R. Zhang, X.B. Wu, Z.X. Dong, Z. Zhu, Y. Yang, *J. Electrochem. Soc.* **155**, A775 (2008).
20. Y.-K. Sun, S.-T. Myung, M.-H. Kim, J. Prakash, K. Amine, *J. Am. Chem. Soc.* **127**, 13411 (2005).
21. Y.-K. Sun, S.-T. Myung, M.-H. Kim, J.-H. Kim, *Electrochem. Solid-State Lett.* **9**, A171 (2006).
22. Y.-K. Sun, S.-T. Myung, H.-S. Shin, Y.C. Bae, C.S. Yoon, *J. Phys. Chem. B* **110**, 6810 (2006).
23. Y.-K. Sun, S.-T. Myung, B.-C. Park, K. Amine, *Chem. Mater.* **18**, 5159 (2006).
24. B.-C. Park, H.J. Bang, K. Amine, E. Jung, Y.-K. Sun, *J. Power Sources* **174**, 658 (2007).
25. K.-S. Lee, S.-T. Myung, Y.-K. Sun, *J. Power Sources* **195**, 6043 (2010).
26. Z.L. Yang, C. Cao, F.F. Liu, D.R. Chen, X.L. Jiao, *Solid State Ionics* **181**, 678 (2010).
27. W.M. Zhang, J.S. Hu, Y.G. Guo, S.F. Zheng, L.S. Zhong, W.G. Song, L.J. Wan, *Adv. Mater.* **20**, 1160 (2008).
28. Z.L. Yang, C. Cao, F.F. Liu, D.R. Chen, X.L. Jiao, *Solid State Ionics* **181**, 678 (2010).
29. M. Jo, Y.K. Lee, K.M. Kim, J. Cho, *J. Electrochem. Soc.* **157**, A841 (2010).
30. X.-L. Wang, M. Feygenson, M.C. Aronson, W.-Q. Han, *J. of Phy. Chem. C* **114**, 14697 (2010).
31. Y.-K. Sun, S.-T. Myung, B.-C. Park, J. Prakash, I. Belharouak, K. Amine, *Nat. Mater.* **8**, 320 (2009).
32. Y.-K. Sun, D.-H. Kim, C.S. Yoon, S.-T. Myung, J. Prakash, K. Amine, *Adv. Funct. Mater.* **20**, 485 (2010).
33. Y.-K. Sun, D.-H. Kim, H.-G. Jung, S.-T. Myung, K. Amine, *Electrochim. Acta* **55**, 8621 (2010).
34. Y.-K. Sun, B.-R. Lee, H.-J. Noh, H. Wu, S.T. Myung, K. Amine, *J. Mater. Chem.* (2011); DOI:10.1039/c0jm04242k.
35. M.S. Bhuwaneswari, L. Dimesso, W. Jaegermann, *J. Sol–Gel Sci. Technol.* **56**, 320 (2010).
36. N. Jayaprakash, N. Kalaiselvi, C.H. Doh, Gangulibabu, D. Bhuvaneswari, *J. Appl. Electrochem.* **40**, 2193 (2010).
37. S. Soltanmohammad, S. Asgari, *J. Nanomater.* Article ID 695083 (2010); DOI:10.1155/2010/104012.
38. K. Nakahara, R. Nakajima, T. Matsushima, H. Majima, *J. Power Sources* **117**, 131 (2003).
39. D. Yoshikawa, Y. Kadoma, J.M. Kim, K. Ui, N. Kumagai, N. Kitamura, Y. Idemoto, *Electrochim. Acta* **55**, 1872 (2010).
40. F. Yu, J.J. Zhang, Y.F. Yang, G.Z. Song, *J. Appl. Electrochem.* **14**, 883 (2010).
41. M.-H. Lee, Y.-J. Kang, S.-T. Myung, Y.-K. Sun, *Electrochim. Acta* **50**, 939 (2004).
42. A.V. Bommel, J.R. Dahn, *J. Electrochem. Soc.* **156**, A362 (2009).
43. J.H. Lim, H.J. Bang, K.S. Lee, K. Amine, Y.K. Sun, *J. Power Sources* **189**, 571 (2009).
44. S.-H. Park, H.-S. Shin, S.-T. Myung, C.S. Yoon, K. Amine, Y.-K. Sun, *Chem. Mater.* **17**, 6 (2005).
45. G.-H. Kim, S.-T. Myung, H.J. Bang, J. Prakash, Y.-K. Sun, *Electrochem. Solid-State Lett.* **7**, A477 (2004).
46. Z.H. Chen, Y. Qin, K. Amine, Y.-K. Sun, *J. Mater. Chem.* **20**, 7606 (2010).
47. Y.-K. Sun, K.-J. Hong, J. Prakash, K. Amine, *Electrochem. Commun.* **4**, 344 (2002).
48. J. Akimoto, Y. Takahashi, N. Kijima, *Electrochem. Solid-State Lett.* **8**, A361 (2005).
49. K. Amine, J. Liu, I. Belharouak, S.H. Kang, I. Bloom, D. Vissers, G. Henriksen, *J. Power Sources* **146**, 111 (2005).
50. W.Q. Lu, Z.H. Chen, H. Joachin, J. Prakash, J. Liu, K. Amine, *J. Power Sources* **163**, 1074 (2007).
51. Z.H. Chen, Y. Qin, J. Liu, K. Amine, *Electrochem. Solid-State Lett.* **12**, A69 (2009).
52. M. Mladenov, R. Stoyanova, E. Zhecheva, S. Vassilev, *Electrochem. Commun.* **3**, 410 (2001).
53. J. Cho, C.S. Kim, S.I. Yoo, *Electrochem. Solid-State Lett.* **3**, 362 (2000).
54. Z.H. Chen, J.R. Dahn, *Electrochim. Acta* **49**, 1079 (2004).
55. S.-T. Myung, K. Izumi, S. Komaba, Y.-K. Sun, H. Yashiro, N. Kumagai, *Chem. Mater.* **17**, 3695(2005).
56. J.-M. Han, S.-T. Myung, Y.-K. Sun, *J. Electrochem. Soc.* **153**, A1290, (2006).
57. Y. Wu, A.V. Murugan, A. Manthiram, *J. Electrochem. Soc.* **155**, A635, (2008).
58. D.Q. Liu, Z.Z. He, X. Liu, *Mater. Lett.* **61**, 4703 (2007).
59. D. Ahn, J.G. Lee, J.S. Lee, J. Kim, J. Cho, B. Park, *Cur. Appl. Phys.* **7**, 172 (2007).
60. S.-T. Myung, K. Izumi, S. Komaba, H. Yashiro, H.J. Bang, Y.-K. Sun, N. Kumagai, *J. Phys. Chem. C* **111**, 4061 (2007).
61. B.J. Hwang, C.Y. Chen, M.Y. Cheng, R. Santhanam, K. Ragavendran, *J. Power Sources* **195**, 4255 (2010).
62. S.H. Kang, J. Kim, M.E. Stoll, D. Abraham, Y.K. Sun, K. Amine, *J. Power Sources* **112**, 41 (2002). □



JANIS

Cryogenic Products for Materials Characterization



Janis has a wide range of products geared towards the materials scientist, covering nearly any temperature range or application.

Typical techniques include: VSM, MOKE, FTIR, ESR, EPR, NMR, Hall effect, DLTS, Mössbauer, STM, AFM and more

Typical applications include:

- Microscopy
- UV-Vis-IR optical measurements
- Nanoscale electronics
- Spintronics
- High frequency measurements
- Non-destructive device and wafer testing
- Photovoltaics
- High Tc superconductors
- Terahertz detectors and devices

Janis Research Company
2 Jewel Drive Wilmington, MA 01887 USA
TEL +1 978 657-8750 FAX +1 978 658-0349 sales@janis.com
Visit our website at www.janis.com

https://doi.org/10.1557/mrs.2011.155 Published online by Cambridge University Press